

Spin state engineering of spinel oxide by integration of Cr doping and p-n junction for water oxidation

Yingxin Ma,^{a,†} Yu Zhang,^{b,†} Mengyuan Xing,^a Sailei Kang,^a Mengmeng Du,^a Bocheng Qiu,^{a*} and Yang Chai^{c*}

Experimental section

Preparation of Cr-Co₃O₄/CC: Typically, 1.0 mmol CoCl₂·6H₂O, 0.5 mmol Cr(NO₃)₃·6H₂O, 15 mmol urea, and 3 mmol NH₄F were dissolved into 80 mL deionized (DI) water under magnetically stirring. After stirring for 30 min, a 4*2 cm carbon cloth (CC) with hydrophilic treatment was immersed into the above solution. After solvothermal treatment at 120 °C for 5 h, the product was washed with DI water for two times, and then was dried at 40 °C for overnight. For the Cr-dopant-free Co₃O₄/CC, the preparation procedure was similar with Cr-Co₃O₄/CC, except that 1.0 mmol CoCl₂·6H₂O, 0.5 mmol Cr(NO₃)₃·6H₂O were replaced by 1.5 mmol CoCl₂·6H₂O. Note that the loading amounts of Cr-Co₃O₄/CC and Co₃O₄/CC is about 0.29 mg/cm².

Preparation of Cr-Co₃O₄@NiFe-LDH/CC: The Cr-Co₃O₄@NiFe-LDH/CC was synthesized via electrodepositing NiFe LDH on the Cr-Co₃O₄/CC in a mixed solution containing 6 mM Ni(NO₃)₂ and 3 mM FeSO₄ under the applied potential of -1.0 V versus Ag/AgCl electrode for 350 s (An ultrasonic treatment with Cr-Co₃O₄/CC for 1 h was required before deposition of NiFe-LDH, which aimed to obtain a similar loading amount of Cr-Co₃O₄@NiFe-LDH (0.3 mg/cm²) relative to that of Cr-Co₃O₄/CC and Co₃O₄/CC). For the synthesis of Co₃O₄@NiFe-LDH/CC, the procedure is similar to that of NiFe-LDH@Cr-Co₃O₄/CC, except that Cr-Co₃O₄/CC is replaced by Co₃O₄/CC. Note that the loading amount of Co₃O₄@NiFe-LDH on CC was controlled at approximately 0.31 mg/cm². The NiFe-LDH/CC was synthesized via electrodepositing NiFe LDH on the CC in a mixed solution containing 12 mM Ni(NO₃)₂ and 6 mM FeSO₄ under the applied potential of -1.0 V versus Ag/AgCl electrode for 350 s, and the loading mass of NiFe-LDH on CC was determined to be approximately 0.28 mg/cm².

Preparation of RuO₂/CC: 5 mg RuO₂ powder was firstly dispersed in 1 mL mixed solvent containing 760 μL of ethanol, 200 μL of DI water and 40 μL of 5 wt% Nafion

solution to form a homogeneous ink. 120 μL ink was homogeneously dropped onto the both sides of CC with $1 \times 1 \text{ cm}^2$ and then dried at $40 \text{ }^\circ\text{C}$. Note that the loading mass of RuO_2 on CC is about 0.3 mg/cm^2 .

Materials characterizations

XRD patterns were recorded in the range from 10° to 80° (2θ) using a Rigaku/MiniFlex600 diffractometer with $\text{Cu } K\alpha$ radiation ($\lambda = 1.5406 \text{ \AA}$), operated at 40 kV and 100 mA. Field-emission scanning electron microscope (FESEM; JEOL 6700), transmission electron microscope (TEM; JEOL2011), and high resolution transmission electron microscope (HRTEM; FEI talos F200x G2) equipped with energy-dispersive X-ray spectroscopy (EDX; Super-X) were employed to examine the morphologies and compositions of all the samples. The instrument employed for XPS studies was a Thermo Scientific K-Alpha system with $\text{Al } K\alpha$ radiation ($h\nu=1486.6 \text{ eV}$) operated at 12 kV. The binding energy shift of all the samples induced by the relative surface charging was corrected using the $\text{C}1\text{s}$ level at 284.6 eV as an internal standard. UV-Vis spectra were carried out on the spectrophotometer (Shimadzu, UV-3600plus). Gas chromatography system (GC-2014C) equipped with a molecular sieve (5 \AA) column and a thermal conductivity detector was used to quantify O_2 amount. The concentrations of metallic elements were determined by inductively coupled plasma mass spectrometry (ICP-MS, Agilent 7700x). MS plots were recorded on an electrochemical workstation (Chenhua, CHI660E) with a standard three electrode cell, in which catalyst grown on CC, Pt wire, and saturated calomel electrode are regarded as working electrode, counter electrode, and reference electrode, respectively. Note that the 0.5 M Na_2SO_4 electrolyte needs to be purged with N_2 for 30 min in advance.

Electrochemical Measurements

The electrochemical activity towards oxygen evolution was performed on an electrochemical workstation (Chenhua, CHI660E) with a three-electrode system. The catalysts grown on the carbon cloth (CC) with a size of $1 \times 1 \text{ cm}^2$, graphite rod, and Hg/HgO (KOH saturated) electrode are used as the working electrode, counter electrode and reference electrode, respectively. Potentials were referenced to a reversible hydrogen electrode (RHE): $E_{\text{RHE}} = E_{\text{Hg/HgO}} + 0.098 + 0.059 \times \text{pH}$. The overpotential (η) was calculated according to the following formula: $\eta = E_{\text{RHE}} - 1.23 \text{ V}$. Linear sweep voltammetry (LSV) was carried out at a scan rate of 5 mV s^{-1} in an O_2 -

saturated 1.0 M KOH. All the LSV data presented were corrected for IR loss. The chronoamperometry curve was recorded at a fixed current density of 100 mA cm⁻². EIS analysis were carried out at the overpotential of 270 mV from 0.1 to 100k Hz with an amplitude of 5 mV. The electrochemical double-layer capacitance (C_{dl} , mF cm⁻²), proportional to the electrochemical surface area (ECSA), was determined from the CV curves measured in a potential range from 0.904 to 0.953 V (E *V*s. RHE) according to the following equation: $C_{dl} = \Delta j / 2v$, where Δj is equal to the anode current (j_a) minus the cathode current (j_c) at the potential of 0.928 V (E *V*s. RHE). The electrochemical surface area (ECSA) of different catalysts is calculated by the following equation: $ECSA = C_{dl} / C_s$, in which C_s is the C_{dl} of the ideally flat electrode and taken as 40 μ F cm⁻² in 1M KOH (Table S3).¹ Assuming that four electrons are required to generate one O₂ molecule, the Faraday efficiency can be calculated as follows: Faraday efficiency = $(4 * n_{O_2} * F) / Q$, where F is the faraday efficiency.

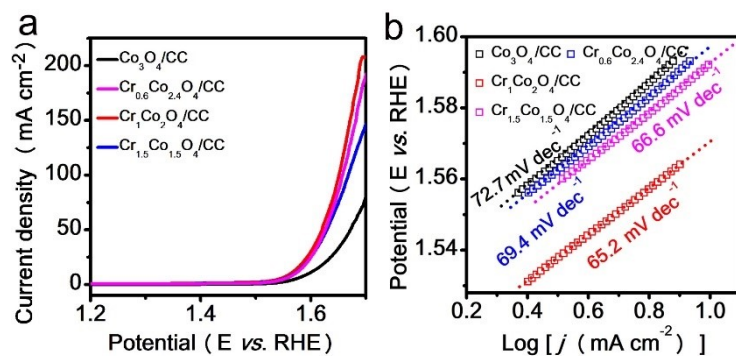


Fig. S1 (a) LSV curves and (b) Tafel slopes of Cr- $\text{Co}_3\text{O}_4/\text{CC}$ with different Cr concentrations. Note that the Cr/Co molar ratio is determined by the feed ratios in the preparation.

The linear sweep voltammetry (LSV) (Fig. S1) shows that $\text{Cr}_1\text{Co}_2\text{O}_4/\text{CC}$ enables the highest OER activity among these samples and the smallest value of Tafel slope, which is indicative of $\text{Cr}_1\text{Co}_2\text{O}_4/\text{CC}$ with best thermodynamic and kinetic properties. In this work, $\text{Cr}_1\text{Co}_2\text{O}_4/\text{CC}$ prepared under the optimal parameters is denoted as Cr- $\text{Co}_3\text{O}_4/\text{CC}$.

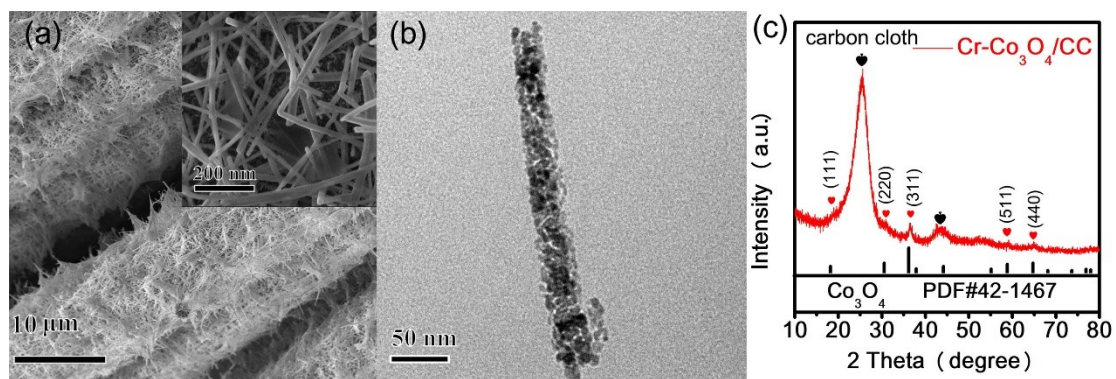


Fig. S2 (a) SEM image, (b) TEM image, and (c) XRD pattern of Cr-Co₃O₄/CC.

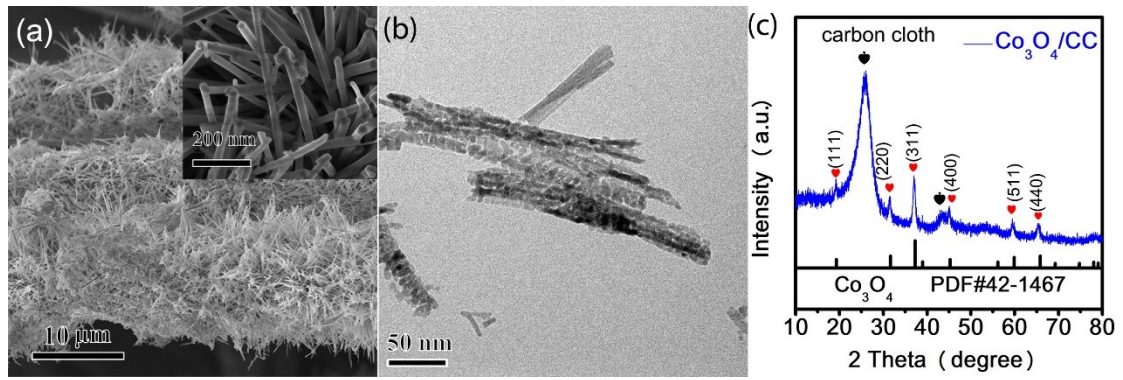


Fig. S3 (a) SEM image, (b) TEM image, and (c) XRD pattern of Co₃O₄/CC.

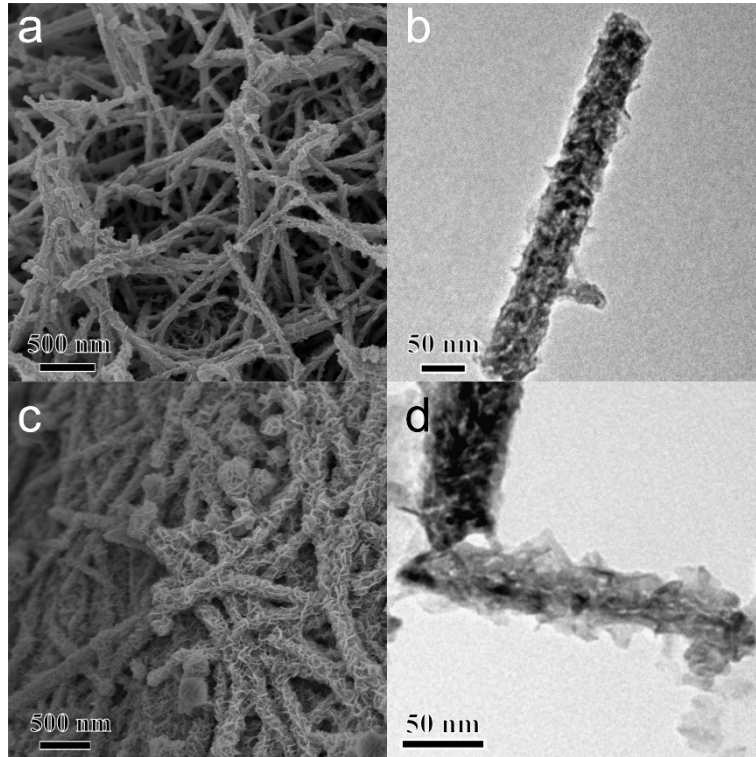


Fig. S4 SEM and TEM images for Cr-Co₃O₄@ NiFe-LDH/CC with different Cr-Co₃O₄/NiFe-LDH ratio via tuning the electrochemical deposition time: (a,b) 150 s and (c,d) 550 s

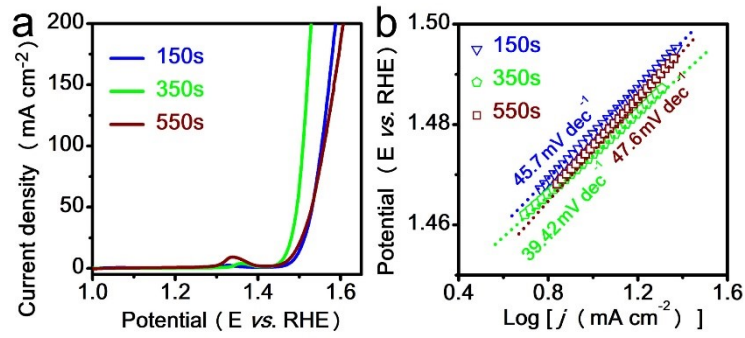


Fig. S5 (a) LSV curves and (b) Tafel slope of Cr-Co₃O₄@NiFe-LDH/CC with different Cr-Co₃O₄/NiFe-LDH ratio via tuning the electrochemical deposition time.

The OER activity of Cr-Co₃O₄@NiFe-LDH/CC with different NiFe-LDH concentrations were evaluated. As shown in Fig. S5, when the electro-deposition time of NiFe-LDH was 350 s, the best thermodynamic and kinetic performances for OER were realized. For clarity, the sample with electrochemical deposition time of 350 s is denoted as Cr-Co₃O₄@NiFe-LDH/CC in this work. The Ni and Fe concentrations in Cr-Co₃O₄@NiFe-LDH/CC were determined to be 15.6 wt% and 7.5 wt% by using ICP-MS, respectively.

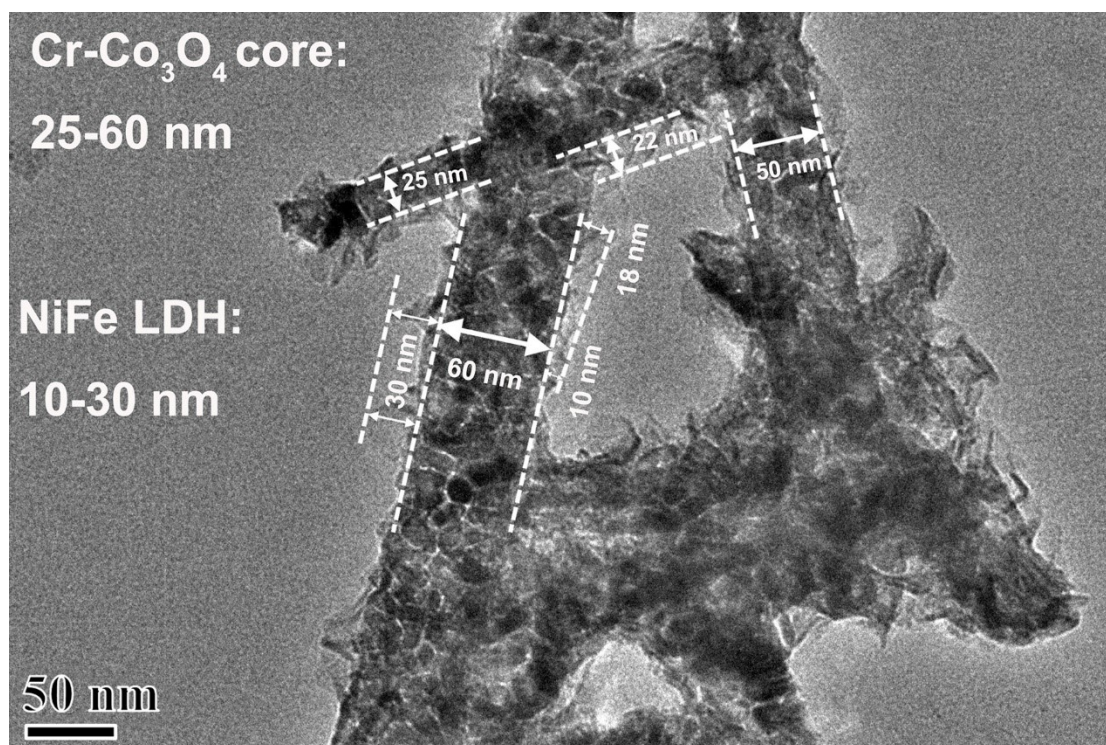


Fig. S6 Statistical data of the sizes of the Cr-Co₃O₄ core and NiFe-LDH shell.

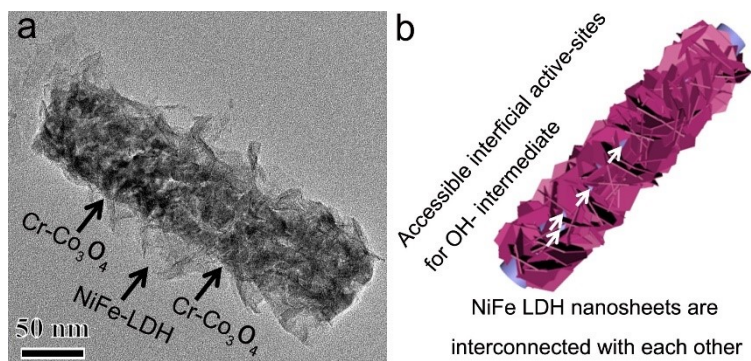


Fig. S7 illustration of interfacial catalytic sites for the adsorption of OH⁻: (a) experimental and (b) theoretical models.

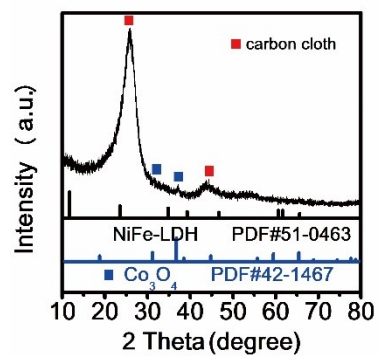


Fig. S8 XRD patterns of Cr-Co₃O₄@NiFe-LDH/CC.

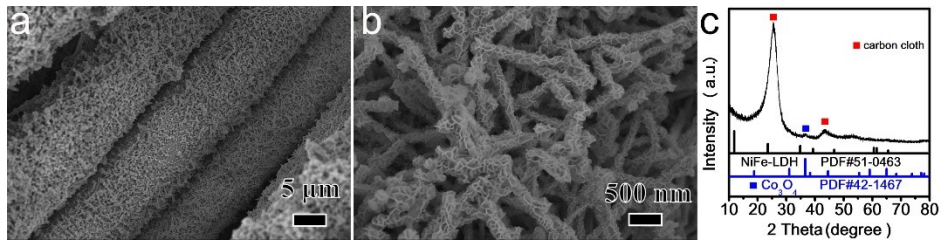


Fig. S9 (a,b) SEM image and (c) XRD pattern of $\text{Co}_3\text{O}_4@\text{NiFe-LDH/CC}$.

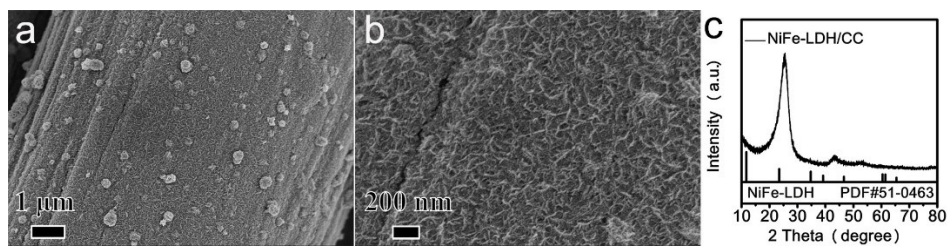


Fig. S10 (a) (a,b) SEM image and (c) XRD pattern of NiFe-LDH/CC.

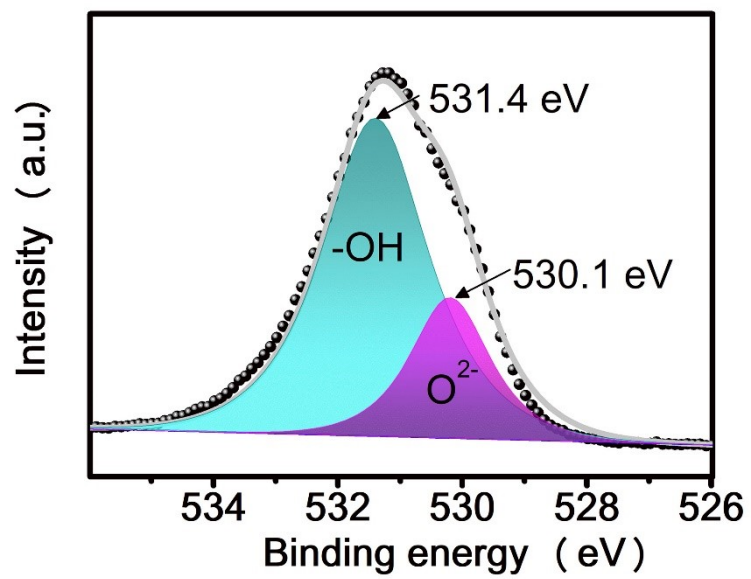


Fig. S11 High resolution O 1s XPS spectrum of Cr-Co₃O₄@NiFe-LDH/CC.

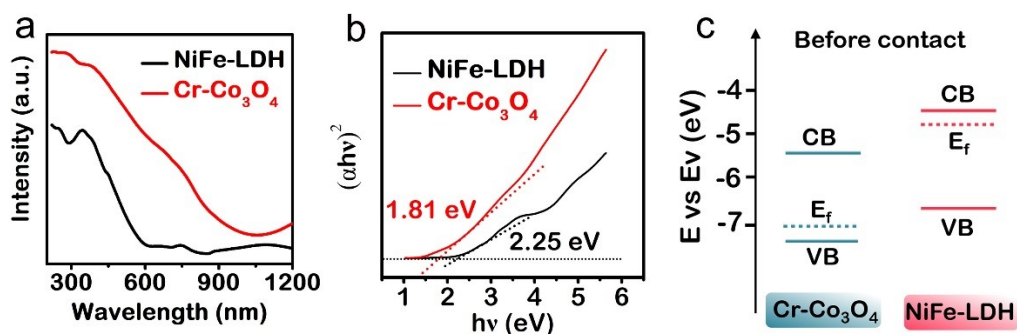


Fig. S12 (a) UV-Vis absorption spectra, (b) the transformed Kubelka-Munk function against the photon energy plot, and (c) energy band alignment of Cr-Co₃O₄ and NiFe-LDH.

Electron volts can be converted to electrochemical energy potentials in volts in terms of the reference standard for which 0 V versus RHE equals -4.44 eV versus vacuum level.² According to this principle, the flat band potential of 1.03 V vs. RHE for Cr-Co₃O₄ (Fig. 2c) is determined to be -5.47 eV vs. vacuum level, while the flat band potential of -0.04 V vs. RHE for NiFe-LDH (Fig. 2d) is determined to be -4.40 eV vs. vacuum level. Moreover, the bandgaps of Cr-Co₃O₄ and NiFe-LDH are calculated to be 1.81 and 2.25 eV via the UV-Vis spectra (Fig. S12a) and the corresponding transformed Kubelka-Munk function (Fig. S12b). As a consequence, the energy level alignments of Cr-Co₃O₄ and NiFe-LDH are proposed in Fig. S12c. Before contact, the obvious differences on Fermi level between Cr-Co₃O₄ and NiFe-LDH can be observed.

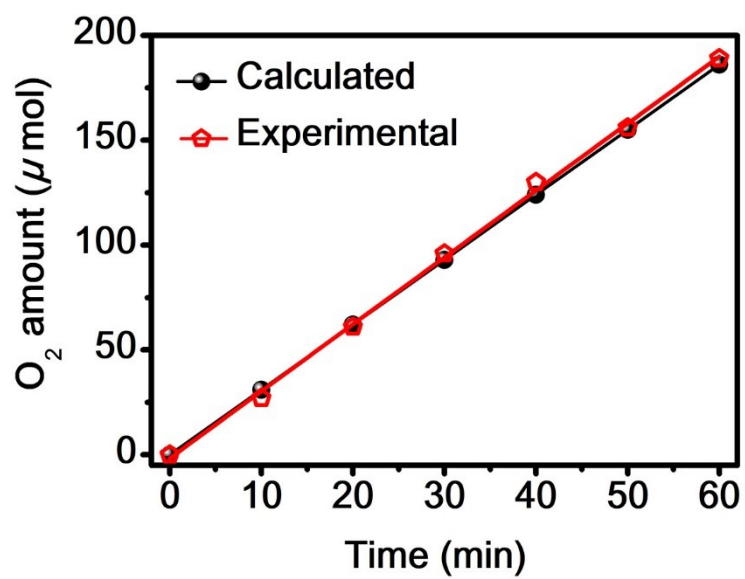


Fig. S13 Calculated versus experimental oxygen evolution over Cr-Co₃O₄@ NiFe-LDH/CC at a constant current of 20 mA.

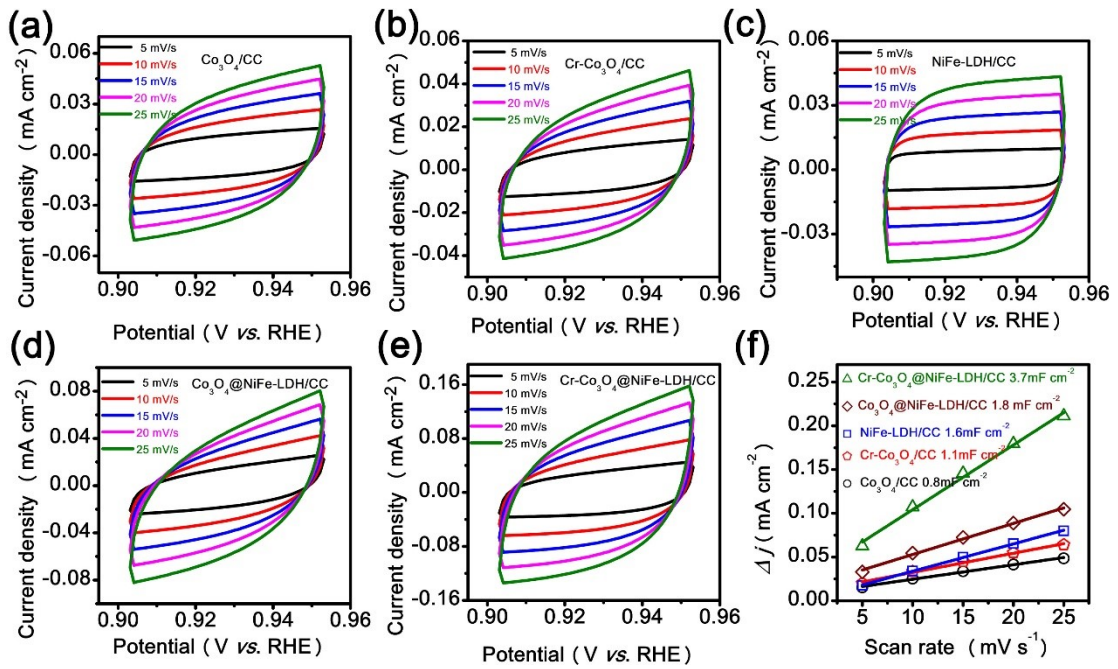


Fig. S14 Cyclic voltammetry curves for (a) Co₃O₄/CC, (b) Cr-Co₃O₄/CC, (c) NiFe-LDH/CC, (d) Co₃O₄@ NiFe-LDH/CC, and (e) Cr-Co₃O₄@ NiFe-LDH/CC.

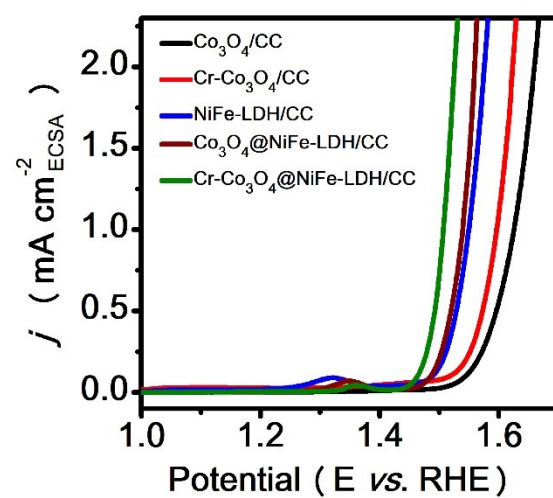


Fig. S15 Normalized specific activities by ECSAs.

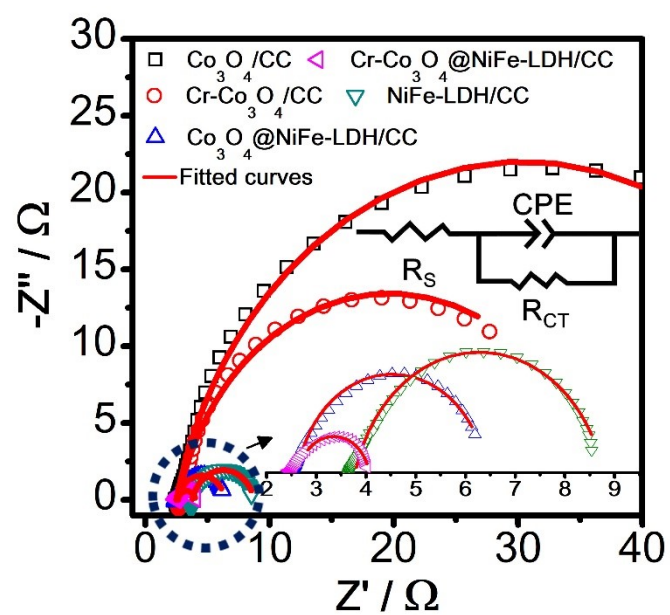


Fig. S16 Nyquist plots of different samples recorded at an overpotential of 270 mV, and the insets are the partially enlarged image and the equivalent circuit model.

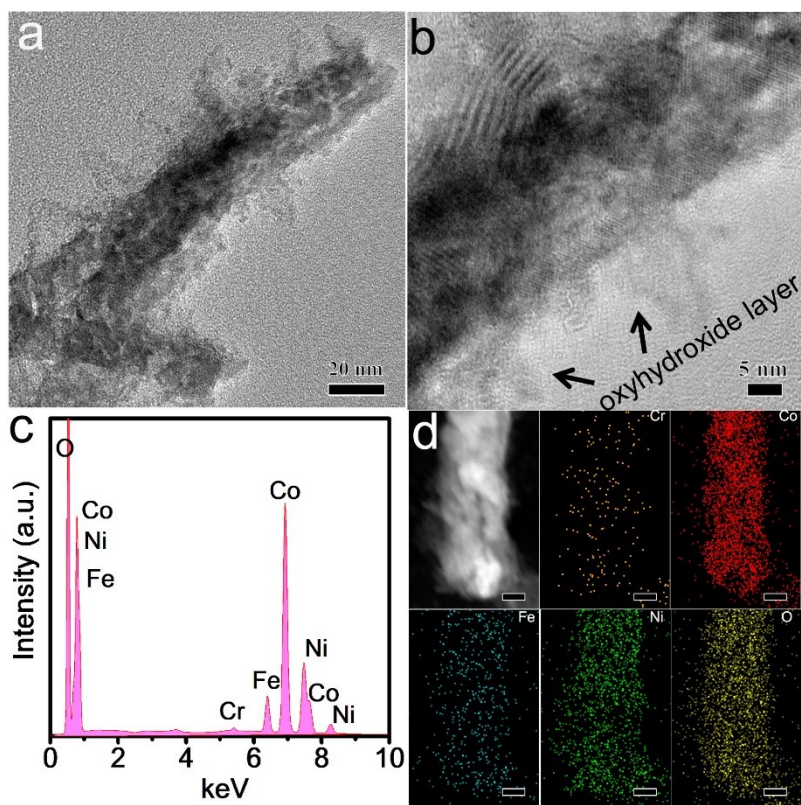


Fig. S17 (a) TEM, (b) HRTEM, (c) EDX spectrum, and (d) element mapping of the recovered Cr-Co₃O₄@ NiFe-LDH/CC after OER.

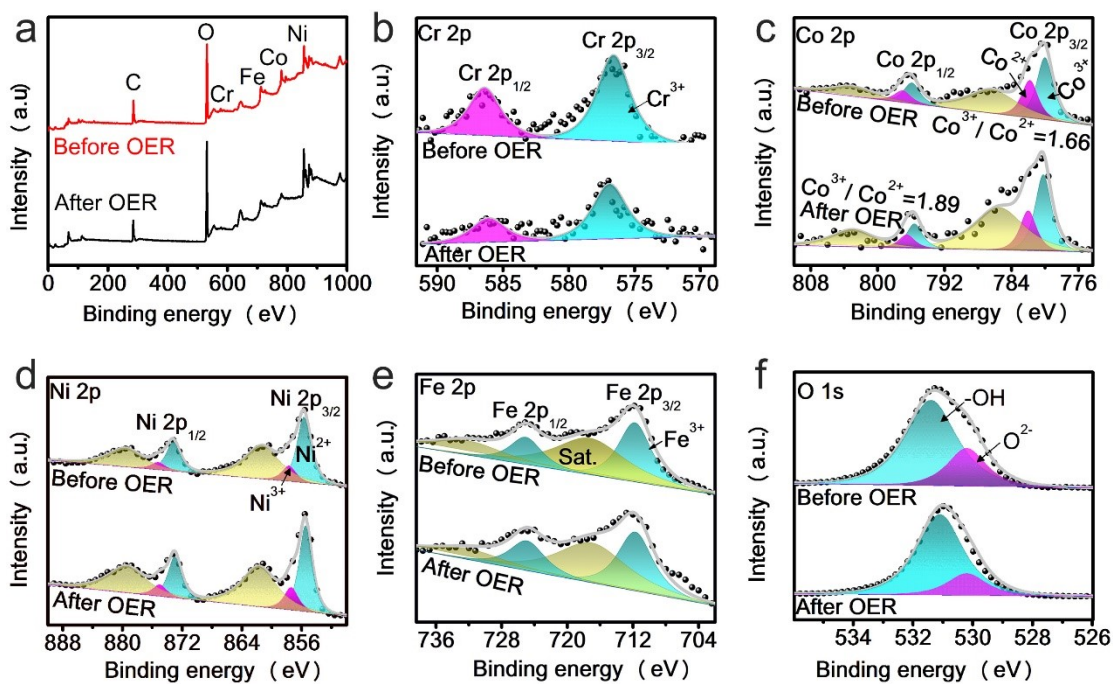


Fig. S18 XPS spectra of (a) survey, (b) Cr 2p, (c) Co 2p, (d) Ni 2p, (e) Fe 2p, and (f) O 1s for Cr-Co₃O₄@NiFe-LDH/CC before and after HER.

a slightly increased Co³⁺/Co²⁺ can be observed (Fig. S18c), indicating that a part of Co²⁺(OH) sites were converted into Co³⁺(OH) sites under a highly oxidized condition. As for other elements, no significant changes in electronic configurations can be observed.

Table S1 Element composition concentrations of different catalysts by using ICP-MS.

Catalysts	Cr (wt%)	Co (wt%)	Ni (wt%)	Fe (wt%)
Cr-Co ₃ O ₄ /CC	11.4	26.7	0	0
Cr-Co ₃ O ₄ @NiFe-LDH/CC before OER	5.4	14.2	15.6	7.5
Cr-Co ₃ O ₄ @NiFe-LDH/CC after OER	2.1	12.3	14.2	7.0

Table S2 Summary of various Co₃O₄-based electrocatalysts for OER performance.

Catalysts	Overpotential (mV) at 10 mA cm ⁻²	Tafel Slope (mV dec ⁻¹)	Ref.
Co ₃ O ₄ /Co-Fe nanoboxes	297	61	Wang <i>et al.</i> ³
Co ₃ O ₄ /NiCo ₂ O ₄ nanocage	340	88	Hu <i>et al.</i> ⁴
Co ₃ O ₄ /NRGO	420	80	Kumar <i>et al.</i> ⁵
Co ₃ O ₄ -MnO ₂ -CNT	390	50	Xie <i>et al.</i> ⁶
NiO/Co ₃ O ₄ @NC	240	73	Tahir <i>et al.</i> ⁷
NiFe-60/Co ₃ O ₄ @NF	190	34.6	Lv <i>et al.</i> ⁸
Au@Co ₃ O ₄	310	60	Zhuang <i>et al.</i> ⁹
M-NiO@Co ₃ O ₄	290	68	Cheng <i>et al.</i> ¹⁰
Co ₃ O ₄ /CeO ₂	279	60	Liu <i>et al.</i> ¹¹
P doped Co ₃ O ₄	280	51.6	Xiao <i>et al.</i> ¹²
Pd@PdO-Co ₃ O ₄ nanocubes	310	78	Li <i>et al.</i> ¹³
Co ₃ O ₄ @MoS ₂	269	58	Liu <i>et al.</i> ¹⁴
CeO ₂ /Co ₃ O ₄	265	68.1	Qiu <i>et al.</i> ¹⁵
Cr-Co ₃ O ₄ @NiFe-LDH/CC	235	39.4	This work.

Table S3 The calculated ECSA values of different samples by taking the C_{dl} and dividing by the general specific capacitances (C_s).

Catalysts	Co ₃ O ₄ /CC	Cr-Co ₃ O ₄ /CC	NiFe-LDH/CC	Co ₃ O ₄ @NiFe-LDH/CC	Cr-Co ₃ O ₄ @NiFe-LDH/CC
ECSA	20	27.5	40	45	92.5

Note that the C_{dl} value is determined to be 40 μF cm⁻² in 1M KOH.

Table S4 The fitted results of the EIS plots.

Catalyst	Co ₃ O ₄ /CC	Cr-Co ₃ O ₄ /CC	NiFe-LDH/CC	Co ₃ O ₄ @NiFe-LDH/CC	Cr-Co ₃ O ₄ @NiFe-LDH/CC
R _s (Ω)	2.7	3.0	3.8	2.6	2.6
R _{CT} (Ω)	54.6	31.1	4.9	3.9	1.4

References

1. C. C. McCrory, S. Jung, J. C. Peters and T. F. Jaramillo, *J. Am. Chem. Soc.*, 2013, **135**, 16977-16987.
2. J. Liu, Y. Liu, N. Liu, Y. Han, X. Zhang, H. Huang, Y. Lifshitz, S.-T. Lee, J. Zhong and Z. Kang, *Science*, 2015, **347**, 970-974.
3. X. Wang, L. Yu, B. Y. Guan, S. Song and X. W. Lou, *Adv. Mater.*, 2018, **30**, 1801211.
4. H. Hu, B. Guan, B. Xia and X. W. Lou, *J. Am. Chem. Soc.*, 2015, **137**, 5590-5595.
5. K. Kumar, C. Canaff, J. Rousseau, S. Arrii-Clacens, T. k. W. Napporn, A. Habrioux and K. B. Kokoh, *J. Phys. Chem. C*, 2016, **120**, 7949-7958.
6. K. Xie, J. Masa, E. Madej, F. Yang, P. Weide, W. Dong, M. Muhler, W. Schuhmann and W. Xia, *ChemCatChem*, 2015, **7**, 3027-3035.
7. M. Tahir, L. Pan, R. Zhang, Y.-C. Wang, G. Shen, I. Aslam, M. Qadeer, N. Mahmood, W. Xu and L. Wang, *ACS Energy Lett.*, 2017, **2**, 2177-2182.
8. J. Lv, L. Wang, R. Li, K. Zhang, D. Zhao, Y. Li, X. Li, X. Huang and G. Wang, *ACS Catal.*, 2021, **11**, 14338-14351.
9. Z. Zhuang, W. Sheng and Y. Yan, *Adv. Mater.*, 2014, **26**, 3950-3955.
10. F. Cheng, X. Fan, X. Chen, C. Huang, Z. Yang, F. Chen, M. Huang, S. Cao and W. Zhang, *Ind. Eng. Chem. Res.*, 2019, **58**, 16581-16587.
11. Y. Liu, C. Ma, Q. Zhang, W. Wang, P. Pan, L. Gu, D. Xu, J. Bao and Z. Dai, *Adv. Mater.*, 2019, **31**, 1900062.
12. Z. Xiao, Y. Wang, Y.-C. Huang, Z. Wei, C.-L. Dong, J. Ma, S. Shen, Y. Li and S. Wang, *Energy Environ. Sci.*, 2017, **10**, 2563-2569.
13. H. C. Li, Y. J. Zhang, X. Hu, W. J. Liu, J. J. Chen and H. Q. Yu, *Adv. Energy Mater.*, 2018, **8**, 1702734.
14. J. Liu, J. Wang, B. Zhang, Y. Ruan, H. Wan, X. Ji, K. Xu, D. Zha, L. Miao and J. Jiang, *J. Mater. Chem. A*, 2018, **6**, 2067-2072.
15. B. Qiu, C. Wang, N. Zhang, L. Cai, Y. Xiong and Y. Chai, *ACS Catal.*, 2019, **9**, 6484-6490.